Hindawi
Wireless Communications and Mobile Computing
Volume 2022, Article ID 2906739, 10 pages
https://doi.org/10.1155/2022/2906739

Research Article

An Effective Scheme of Building Electromagnetic Map for Spectrum Sensing

Dongming Lin,[1] **Hongjun Wang**,[1] **Zhi Lin**,[1] **Kang An**,[2] **Zhexian Shen**,[1] **and Jiangzhou Wang**[3]

[1]*College of Electronic Engineering, National University of Defense Technology, Hefei 230037, China*
[2]*Sixty-Third Research Institute, National University of Defense Technology, Nanjing 210007, China*
[3]*School of Engineering, University of Kent, Canterbury CT2 7NZ, UK*

Correspondence should be addressed to Hongjun Wang; hongjun-wang@163.com

Received 27 May 2022; Accepted 28 June 2022; Published 25 July 2022

Academic Editor: Mingqian Liu

To address the severe spectrum scarcity problem and achieve efficient green communications, we propose a new and practical scheme to obtain electromagnetic data (ED) and a composite electromagnetic map reconstruction method (CEMRM). The scheme uses a small number of sensing nodes to obtain incomplete sampled ED, then uses CEMRM to reconstruct complete ED according to the incomplete ED and builds realistic electromagnetic maps (EMs) in various propagation scenarios. Specifically, we firstly adopt kriging (KG) method to obtain the geography-based ED (GED) according to geographical correlation of the locations of the sampled ED. Meanwhile, a novel algorithm, named filtered subdistrict sparsity adaptive matching pursuit (FSSAMP), is proposed to obtain the pure ED (PED) according to electromagnetic correlation of the sampled ED. Then, weight factors are mapped into the above two types of data and the fast gradient projection (FGP) method is employed to obtain the highly accurate combined ED (CED). Based on the CED, the accurate and practical EMs can be drawn. Simulation results demonstrate that the proposed scheme can provide more accurate ED and EMs than existing benchmark schemes in various propagation scenarios, and the built EMs can provide accurate information for the assessment of spectrum resources utilization to make spectrum resources efficiently used.

1. Introduction

The rapid development of wireless applications and blossoming growth of traffic demand lead to severe spectrum scarcity problem. To achieve efficient application of spectrum resources and green communications, it is necessary to obtain electromagnetic data (ED) first and then assess the spectrum resources utilization so as to adopt spectrum resources allocation method. In the existing methods to obtain ED, manual measurements cost highly especially in a large-scale area. Employing lots of human beings to obtain the ED is not realistic, and the obtained ED may be not accurate due to the human subjectivity. With the development of automation technology, sensing nodes replace human beings to obtain the ED [1]. However, the cost and effect are relative to the number of sensing nodes. If sensing nodes are deployed redundantly, the cost is high but accurate and complete ED can be obtained. If there are a small number of available sensing nodes deployed, the cost is greatly less than that when sensing nodes are deployed redundantly, and the obtained ED are accurate but incomplete [2]. However, the incomplete ED cannot provide sufficient information for assessing the usage of spectrum resources. The completeness degree of ED and cost are both proportional to the number of sensing nodes in a certain range. The mentioned three types of measurement methods cannot make a balance between the cost and effect. Therefore, it is necessary to study an effective and low-cost method to obtain ED.

An electromagnetic map (EM) [3] is a promising tool for assessing the usage of spectrum resources, which contains lots of information about electromagnetic spectrum resources. The EM can make spectrum resources efficiently

used, which can solve the spectrum scarcity problem and achieve efficient green communications. The existing works on EMs are mainly about the constructing methods of radio environment maps (REMs), whose methods can be classified into three categories, which are called indirect methods, direct methods, and hybrid methods. Indirect methods are mainly based on propagation models or radiation geographical positions, direct methods are mainly interpolation methods, and hybrid methods are the combination of indirect methods and direct methods.

In indirect methods, the authors of [4] proved that the propagation model can be used to construct the REM. ED of unsampled positions can be inferred from the known or estimated radiation source locations and the propagation model, and it is the main method used by the indirect methods to obtain the ED. However, the single electromagnetic propagation model cannot fit the dynamic electromagnetic environment, and the selection of relevant parameters is difficult without relevant information of electromagnetic environment, so the effect of the method based on the propagation model cannot be ensured in the dynamic and noncooperative electromagnetic environment [5, 6].

On the other hand, the direct methods need no information about electromagnetic environment especially propagation models, and they are used to reconstruct the ED according to the geographical correlation of the sampled positions. The kriging (KG) [7] is the mostly used algorithm, and its accuracy is satisfactory [8]. However, the accuracy of KG is influenced by the outliers [9], and the calculation complexity is high [10]. Different from KG, other interpolation methods are used to construct the REM, such as the local polynomial (LP) algorithm [11], nearest neighbour (NN) algorithm [12], and inverse distance weighting (IDW) algorithm [13]. However, LP is sensitive to neighbourhood distance, and a small searching neighbourhood distance will cause an empty hole in the data reconstruction. The data reconstruction result of NN is not continuous. IDW is sensitive to isolating outliers, and a lot of isolating outliers cause downfall in the accuracy when IDW is used in large-scale data reconstruction. Generally, the REM construction effect of existing interpolation methods is relatively lower when the number of sensing nodes is small [8].

In hybrid methods, the mostly used combination scheme is to combine the KG and propagation models [14, 15]. In fact, the combination of a single propagation model and KG is suitable for the special scenario, and the accuracy is much better than KG and the propagation model. However, the effect of the method is relatively lower in scenarios of other kinds of propagation models, and the methods also need information about propagation models in a certain content.

In the case of noncooperation, the information of the electromagnetic environment like propagation models cannot be obtained, even though some methods like maximum likelihood estimation [16] can be used to estimate the information, the error is not acceptable; moreover, the method based on a single propagation model cannot do well in scenarios of different propagation models. In the case that a small number of sensing nodes are available, the interpolation methods cannot obtain good results, and the accuracy needs improvement. As for the hybrid methods, these kinds of methods do badly in the case of noncooperation or the case that a small number of sensing nodes are available, and the method has high complexity. In order to achieve the reconstruction of EMs in the case of noncooperation and the case that a small number of sensing nodes are available, it is necessary to study an effective method.

To address the above challenges, this paper proposed a novel scheme to obtain accurate ED, reconstruct the practical electromagnetic signal map (which we refer to as an EM), and take the reference signal receiving power (RSRP) as the research object of EMs.

The contributions of the paper are summarized as follows:

(1) To achieve ED reconstruction, this paper proposes an improved sparsity adaptive matching pursuit (SAMP) algorithm, which reconstructs ED based on the electromagnetic correlation of the sampled ED. Besides, the processing time of the proposed improved SAMP is much less than that of the traditional SAMP algorithm

(2) To achieve the reconstruction of EMs in the noncooperation situation with a small number of sensing nodes, this paper proposes a composite EM reconstruction method (CEMRM) to obtain the complete and accurate ED and reconstruct realistic EMs. Simulation results show that the obtained EMs reconstructed by the CEMRM are more accurate than those reconstructed by existing methods

The organization of this paper is as follows. Section 2 describes the system model of the proposed scheme. Section 3 presents algorithm description about the proposed method. In Section 4, simulation results are presented. Finally, the paper draws the conclusions in Section 5.

2. System Model

Assuming that there are three base stations in the target area as shown in Figure 1, a small number of sensing nodes are deployed randomly in the target area, and the ratio of sensing nodes to the total number of ED is 2% (smaller than that in existing works [17]). First of all, the target area is divided into grids to ascertain the total number of ED and obtain the corresponding geographic positions. The values of ED are RSRP values. We just consider the electromagnetic datum in each grid center. When reconstructing a large-area EM, the total number of ED is huge. If we study the relation between the change in the specific quantities of sensing nodes and the accuracy of reconstructed EMs, the workload is huge and results are not accurate. However, if we study the relation between the change in the ratio of sensing nodes to the total number of ED and the accuracy of reconstructed EMs, the useless work can be decreased and the results are accurate. Therefore, this paper uses the ratio to describe the number of sensing nodes instead of the specific

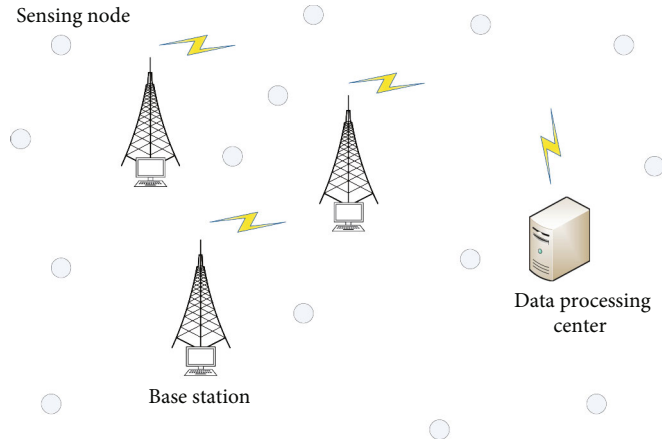

Figure 1: System model. The sketch of the proposed scheme to obtain the ED.

quantities. The sampled ED must be incomplete. After sampling the ED [18, 19], the incomplete data are sent to the data processing center, where CEMRM is adopted to reconstruct the precise EMs. The data processing center assesses the usage of spectrum resources according to the reconstructed EMs and then controls the working status of the base stations with the adopted spectrum resources allocation method. If the data processing center breaks down, the calculating task will be undertaken by the distributed calculating platform in the sensing nodes.

3. Algorithm Description

This section proposes the CEMRM to achieve ED reconstruction, which is shown in Figure 2.

Specifically, CEMRM consists of four parts. In the first part, KG is used to reconstruct the ED according to the incomplete data obtained by sensing nodes, and the obtained geography-based ED (GED) contain strong geographical correlation. At the same time, the filtered subdistric sparsity adaptive matching pursuit (FSSAMP) is used to reconstruct the ED according to the incomplete data obtained by sensing nodes, and the obtained pure ED (PED) contain strong electromagnetic correlation. The ED are affected by geography just in a certain extent, so the GED obtained by KG can be more accurate after being processed with the electromagnetic correlation. In order to make obtained ED containing both geographical and electromagnetic correlation, weight allocation is used to balance the two kinds of correlation.

$$\boldsymbol{G} = 0.8 \times \mathrm{GED} + 0.2 \times \mathrm{PED}. \tag{1}$$

After weight allocation, the primary ED, $\boldsymbol{G}$ is obtained. The fast gradient projection (FGP) is an algorithm to improve the data accuracy according to the correlation of data, so the FGP is promising to help improve the accuracy of the primary ED according to the weight allocation of the geographical and electromagnetic correlation. After $\boldsymbol{G}$ with strong correlation being processed by the FGP, more accurate combined ED (CED) can be obtained. Finally, the EM is drawn with isomagnetic lines according to the CED.

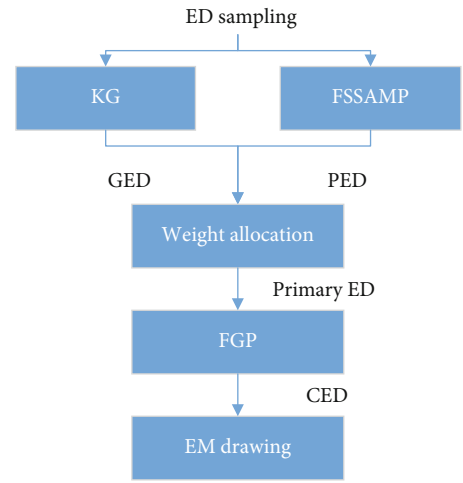

Figure 2: The structure of the proposed CEMRM. GED are the ED reconstructed by KG, PED are the ED reconstructed by FSSAMP.

The proposed CEMRM needs no electromagnetic information about the electromagnetic environment, and it just needs a small number of sensing nodes. With the help of electromagnetic correlation extracted by the FSSAMP, and accuracy improvement by the FGP, it can overcome the weakness that KG is sensitive to outliers and obtain realistic results.

3.1. Kriging. KG is an accurate interpolation algorithm and can reconstruct ED according to geographical correlation, and the obtained ED contain geographical correlation. The principal of KG to predict the RSRP is given by [7].

$$v_{\mathrm{out}}(\boldsymbol{h}) = \mathbf{w}^{\mathrm{T}}(\boldsymbol{h})\boldsymbol{\iota} + e(\boldsymbol{h}), \tag{2}$$

where $v_{\mathrm{out}}(\boldsymbol{h})$ is the value of the RSRP, and $\boldsymbol{h}$ is the location. $\mathbf{w}(\boldsymbol{h}) = [w_1(\boldsymbol{h}), w_2(\boldsymbol{h}), \cdots, w_N(\boldsymbol{h})]^{\mathrm{T}}$ is the vector containing N selected functions that consist of the regression model. $\boldsymbol{\iota} = [\iota_1, \iota_2, \cdots, \iota_N]^{\mathrm{T}}$ is the parameter vector of the model. $e(\boldsymbol{h})$

is a stochastic process satisfying the following conditions:

$$\begin{aligned} E[e(\boldsymbol{h})] &= 0, \\ E\left[e(\boldsymbol{h}_i)e\left(\boldsymbol{h}_j\right)\right] &= \tau^2 R\left(\boldsymbol{\kappa}, \boldsymbol{h}_i, \boldsymbol{h}_j\right), \end{aligned} \tag{3}$$

where $E[\cdot]$ is an operation that calculates the expectation, $\boldsymbol{h}_i$, $\boldsymbol{h}_j$ are both input locations, $R(\boldsymbol{\kappa}, \boldsymbol{h}_i, \boldsymbol{h}_j)$ is the correlation model, τ^2 is the variance of $e(\boldsymbol{h})$, and $\boldsymbol{\kappa}$ is the parameter of the correlation model. The algorithm defines $[\boldsymbol{b}_1, \cdots, \boldsymbol{b}_q]$ as a set of sampling point locations whose value is $\mathbf{V} = [v_1, \cdots, v_q]^{\mathrm{T}}$. Then,

$$\begin{aligned} \widehat{\boldsymbol{\iota}} &= \left(\mathbf{F}^{\mathrm{T}}\mathbf{R}^{-1}\mathbf{F}\right)^{-1}\mathbf{F}^{\mathrm{T}}\mathbf{R}^{-1}\mathbf{V}, \\ \widehat{\tau}^2 &= \frac{1}{q}\left(\mathbf{V} - \mathbf{F}\widehat{\boldsymbol{\iota}}\right)^{\mathrm{T}}\mathbf{R}^{-1}\left(\mathbf{V} - \mathbf{F}\widehat{\boldsymbol{\iota}}\right), \end{aligned} \tag{4}$$

where $\widehat{\boldsymbol{\iota}}$ and $\widehat{\tau}^2$ are the predicted values of the corresponding variables $\boldsymbol{\iota}$ and τ^2. $\mathbf{F}$ is a $q \times N$ matrix containing $\mathbf{w}(\boldsymbol{b}_i)$, for $i \in [1, q]$. $\mathbf{R}$ is a $q \times q$ correlation matrix of the sampling points containing $R_{ij} = R(\boldsymbol{\kappa}, \boldsymbol{b}_i, \boldsymbol{b}_j)$. The correlation function is defined as follows:

$$R(\boldsymbol{\kappa}, \boldsymbol{\mu}, \boldsymbol{h}) = \prod_{j=1}^{n} R_j\left(\boldsymbol{\kappa}, \mu_j - h_j\right), \tag{5}$$

where n is the dimension of sampling points. Note that the following condition should be ensured:

$$\min_{\boldsymbol{\kappa}}\left[\Lambda(\boldsymbol{\kappa}) = |\mathbf{R}|^{(1/q)}\tau^2\right], \tag{6}$$

where $|\cdot|$ calculates the determinant of a matrix. Here, the spherical model is adopted.

$$R_j\left(\boldsymbol{\kappa}, d_j\right) = 1 - 1.5\xi_j + 0.5\xi_j^3 \quad \xi_j = \min\left\{1, \kappa_j\left|d_j\right|\right\}, \tag{7}$$

where $d_j = \mu_j - h_j$. Then, the predicted RSRP v_{out} of the unsampled location $\boldsymbol{h}$ is shown as follows:

$$\begin{aligned} \widehat{v}_{\mathrm{out}}(\boldsymbol{h}) &= \mathbf{w}^{\mathrm{T}}(\boldsymbol{h})\widehat{\boldsymbol{\iota}} + \mathbf{r}^{\mathrm{T}}(\boldsymbol{h})\mathbf{R}^{-1}\left(\mathbf{V} - \mathbf{F}\widehat{\boldsymbol{\iota}}\right), \\ \mathbf{r}(\boldsymbol{h}) &= \left[R(\boldsymbol{\kappa}, \boldsymbol{h}, \boldsymbol{b}_1), \cdots, R\left(\boldsymbol{\kappa}, \boldsymbol{h}, \boldsymbol{b}_q\right)\right]^{\mathrm{T}}. \end{aligned} \tag{8}$$

The complete ED obtained by the KG are $\mathrm{GED} = \widehat{\mathbf{v}}_{\mathrm{out}}$, where $\widehat{\mathbf{v}}_{\mathrm{out}}$ is the union of $\widehat{v}_{\mathrm{out}}(\mathbf{h})$.

3.2. Improved Sparsity Adaptive Matching Pursuit. The procedure of sampling ED with sensing nodes can be described as

$$\boldsymbol{y} = \boldsymbol{K}\boldsymbol{x}, \tag{9}$$

where $\boldsymbol{y} = [\cdots, 0, y_1, \cdots, 0, y_M, \cdots]^{\mathrm{T}}$ is the sampled ED containing M non-zero values, $\boldsymbol{x}$ is the real complete ED, $\boldsymbol{x} \in R^N$, and $M \ll N$ need to be met. Here, $\boldsymbol{K}$ is the observation matrix.

$$\boldsymbol{K} = \begin{bmatrix} \ddots & & & & \\ & 1 & & & \\ & & \ddots & & \\ & & & 0 & \\ & & & & \ddots \end{bmatrix}_{N \times N}, \tag{10}$$

where N is the total number of ED.

Since it is difficult to determine $\boldsymbol{x}$ directly, the problem is converted to

$$\begin{aligned} &\min \|\boldsymbol{\theta}\|_{l_0}, \\ &\text{s.t.} \quad \boldsymbol{y} = \boldsymbol{A}\boldsymbol{\theta}, \end{aligned} \tag{11}$$

where $\boldsymbol{A} = \boldsymbol{K}\boldsymbol{\Psi}$ is the sensing matrix, $\boldsymbol{\Psi}$ is the sparse base matrix, $\|\cdot\|_{l_0}$ is calculating the l_0-norm of a matrix, and $\boldsymbol{\theta}$ is the projection result of $\boldsymbol{x}$ in the sparse base matrix $\boldsymbol{\Psi}$, which is given by

$$\boldsymbol{\Psi} = \sqrt{N}\begin{bmatrix} 1 & 1 & \cdots & 1 \\ 1 & W_N^1 & \cdots & W_N^{N-1} \\ 1 & W_N^2 & \cdots & W_N^{2(N-1)} \\ \vdots & \vdots & & \vdots \\ 1 & W_N^{N-1} & \cdots & W_N^{(N-1)(N-1)} \end{bmatrix}_{N \times N}, \tag{12}$$

where $W_N = e^{((-j2\pi)/N)}$.

In order to solve Eq. (11), we improve the SAMP [20]. Firstly, the target area is divided into four parts, which are numbered as $\alpha \in [1, 2, 3, 4]$, and a certain number of sensing nodes are randomly deployed in four subareas, respectively. The number of sensing nodes in each subarea is same. Then, the algorithm reconstructs ED of each part parallelly or serially, and then they are integrated into a set of complete ED. Finally, the obtained complete ED are filtered by a median filter. The improved algorithm is summarized as follows.

Needed parameter: the sensing matrix $\boldsymbol{A}$, sampling ED $\boldsymbol{y}$ of the subarea, the step size $s = 4$, which is the number of subareas, and the observation matrix that being changed into the column vector format $\boldsymbol{K}$.

Step 1. Initialize parameters, the residual error $\boldsymbol{r_0} = \boldsymbol{y}$, index matrix $\boldsymbol{H_0} = \varnothing$, the element number $L = s$, $t = 1$, t is the iteration, $\boldsymbol{a}_j$ is the jth column of $\boldsymbol{A}$, stage index std = 1, $\widehat{\boldsymbol{\theta}} = 0_{N \times 1}$.

Step 2. $Y = \mathrm{abs}(\boldsymbol{A}^{\mathrm{T}}\boldsymbol{r_{t-1}})$ is calculated, and the algorithm chooses L maximum values, and obtains a union set ϱ_k containing the column codes of chosen values in $\boldsymbol{A}$.

Step 3. $C_k = \boldsymbol{H_{t-1}} \bigcup \varrho_k$, $\boldsymbol{A}_t = [\boldsymbol{a}_j], j \in C_k$.

Step 4. Least squares solution $\widehat{\boldsymbol{\theta}}_t = \left(\boldsymbol{A}_t^{\mathrm{T}}\boldsymbol{A}_t\right)^{-1}\boldsymbol{A}_t^{\mathrm{T}}\boldsymbol{y}$.

Step 5. The L elements with the biggest absolute values are chosen from $\widehat{\boldsymbol{\theta}}_{\boldsymbol{t}}$, and the corresponding column vectors of the chosen values in $\boldsymbol{A}_t$ make up $\boldsymbol{A}_{t/L}$, the corresponding column codes of the chosen values are$\boldsymbol{H}_{t/L}$.

Step 6. The new residual error $\mathbf{r}_{tc}$ is updated. $\widehat{\boldsymbol{\theta}}_{\boldsymbol{t}} = (\boldsymbol{A}_{t/L}^{\mathrm{T}}\boldsymbol{A}_{t/L})^{-1}\boldsymbol{A}_{t/L}^{\mathrm{T}}\boldsymbol{y}$, $\boldsymbol{r}_{tc} = \boldsymbol{y} - (\boldsymbol{A}_{t/L}\widehat{\boldsymbol{\theta}}_{\boldsymbol{t}})$.

Step 7. If $\|\boldsymbol{r}_{tc}\|_2 < 0.001$ which is $\|\boldsymbol{r}_{tc}\|_2 = 0$ in the original algorithm, $\boldsymbol{H}_t = \boldsymbol{H}_{t/L}$, and do Step 8 directly. If $\|\boldsymbol{r}_{tc}\|_2 \geq \|\boldsymbol{r}_{t-1}\|_2$, $\mathrm{std} = \mathrm{std} + 1$, $L = \mathrm{std} \times s$, $\boldsymbol{r}_t = \boldsymbol{r}_{t-1}, t = t + 1$, and return Step 2; at the same time, if the algorithm reaches the maximum iterations, $\boldsymbol{H}_t = \boldsymbol{H}_{t/L}$ and do Step 8. Or $\boldsymbol{H}_t = \boldsymbol{H}_{t/L}$, $\boldsymbol{r}_t = \boldsymbol{r}_{tc}$, $t = t + 1$ and return Step 2.

Step 8. Update $\widehat{\boldsymbol{\theta}}$, the values whose positions are $\boldsymbol{H}_t$ in $\widehat{\boldsymbol{\theta}}$ is $\widehat{\boldsymbol{\theta}}_{\boldsymbol{t}}$.

Step 9. The corresponding ED of the sub area are $\boldsymbol{\Psi}\widehat{\boldsymbol{\theta}} \times (\boldsymbol{I} - \boldsymbol{K}) + \boldsymbol{y}$, $\boldsymbol{I}$ is the column vector made up of 1.

Step 10. A set of complete ED are obtained by data fusion, which are described as $\hat{\boldsymbol{y}}_o = \mathrm{Union}(\boldsymbol{\Psi}_\alpha\widehat{\boldsymbol{\theta}}_\alpha \times (\boldsymbol{I} - \boldsymbol{K}_\alpha) + \boldsymbol{y}_\alpha)$, $\alpha \in [1, 2, 3, 4]$. The complete ED obtained by the FSSAMP are $\mathrm{PED} = \mathrm{Filter}(\hat{\boldsymbol{y}}_o)$, where Union means the union of the data, $\boldsymbol{\Psi}_\alpha\widehat{\boldsymbol{\theta}}_\alpha \times (\boldsymbol{I} - \boldsymbol{K}_\alpha) + \boldsymbol{y}_\alpha$ is the ED of the corresponding subarea, $\|\cdot\|_2$ calculates the 2-norm of a matrix, and Filter is the median filter.

The median filtering is a kind of nonlinear filtering, and its principle is like

$$\begin{bmatrix} e_1 & e_2 & e_3 \\ e_4 & e_5 & e_6 \\ e_7 & e_8 & e_9 \end{bmatrix}_{3\times 3}, \tag{13}$$

where e_5 is set as the median value of e_1, e_2, e_3, e_4, e_5, e_6, e_7, e_8, and e_9; the values of $e_1 \sim e_9$ are known.

The median filtering can protect the edge information of ED and reduce the influence of isolating outliers, which can help to obtain more accurate results.

3.3. Fast Gradient Projection. The FGP is a good method using the data correlation to increase the precision of data. After the data obtained by Eq. (1) being processed by the FGP, more precise data can be obtained. The accuracy improvement of the FGP is described as a minimum optimization problem, which satisfies

$$\min_{\boldsymbol{E}} J(\boldsymbol{E}) = \frac{1}{2}\|\boldsymbol{E} - \boldsymbol{G}\|_2^2 + \varsigma \boldsymbol{TV}(\boldsymbol{E}), \tag{14}$$

$\|\cdot\|_2$ represents calculating the 2-norm of the matrix, $\boldsymbol{G}$ is the ED obtained by weight allocation, $\boldsymbol{E}$ is more precise ED which is the final result, and $\boldsymbol{TV}(\boldsymbol{E})$ is the total variation regularizer of $\boldsymbol{E}$, ς is the regularization parameter. The dimensions of $\boldsymbol{G}$ and $\boldsymbol{E}$ are both $ii \times jj$.

Table 1: The average running time results of the proposed improved SAMP (FSSAMP) and SAMP.

Type	FSSAMP	SAMP
Time/s	87.9546	1242.3315

In order to solve Eq. (14), we adopt the FGP, which is proposed in [21]. The procedure is given as follows.

First of all, parameters are initialized as $(\boldsymbol{D}_1, \boldsymbol{B}_1) = (\boldsymbol{c}_0, \boldsymbol{m}_0) = (\boldsymbol{0}_{(ii-1)\times jj}, \boldsymbol{0}_{ii\times(jj-1)})$, and $t_1 = 1$.

Then, it is an iterative procedure, in the step $p \in [1, N']$, the algorithm calculates

$$\begin{aligned} (\boldsymbol{c}_p, \boldsymbol{m}_p) &= U_{\ddot{\mathrm{y}}}\left\{(\boldsymbol{D}_p, \boldsymbol{B}_p) + \frac{1}{8\varsigma}\mathfrak{R}^T\left(U_O\left[G - \varsigma\mathfrak{R}(\boldsymbol{D}_p, \boldsymbol{B}_p)\right]\right)\right\}, \\ t_{p+1} &= \frac{1 + \sqrt{1 + 4t_p^2}}{2}, \\ (\boldsymbol{D}_{p+1}, \boldsymbol{B}_{p+1}) &= (\boldsymbol{c}_p, \boldsymbol{m}_p) + \left(\frac{t_p - 1}{t_{p+1}}\right)(\boldsymbol{c}_p - \boldsymbol{c}_{p-1}, \boldsymbol{m}_p - \boldsymbol{m}_{p-1}), \end{aligned} \tag{15}$$

where N' represents the total number of iterations; $\boldsymbol{c}_p$ represents the $\boldsymbol{c}$ in the pth iteration; $\boldsymbol{m}_p$ represents the $\boldsymbol{m}$ in the p th iteration; $\boldsymbol{D}_p$ represents the $\boldsymbol{D}$ in the pth iteration; and $\boldsymbol{B}_p$ represents the $\boldsymbol{B}$ in the pth iteration.

Finally, the more precise result $\boldsymbol{E}$ can be obtained.

$$\boldsymbol{E} = U_O[G - \varsigma\mathfrak{R}(\boldsymbol{c}_{N'}, \boldsymbol{m}_{N'})], \tag{16}$$

where $\boldsymbol{c}_{N'}$ and $\boldsymbol{m}_{N'}$ are obtained in the final iteration.

As a set of matrix pairs, ÿ consists of $(\boldsymbol{c}, \boldsymbol{m})$. The dimension of $\boldsymbol{c}$ is $(ii - 1) \times jj$, $\boldsymbol{m}$ is $ii \times (jj - 1)$, and they satisfy

$$\begin{aligned} c_{l,n}^2 + m_{l,n}^2 &\leq 1, \quad l = 1, \cdots, ii - 1\,; n = 1, \cdots, jj - 1, \\ \left|c_{l,jj}\right| &\leq 1, \quad l = 1, \cdots, ii - 1, \\ \left|m_{ii,n}\right| &\leq 1, \quad n = 1, \cdots, jj - 1, \end{aligned} \tag{17}$$

where $\mathfrak{R}$ is an operation that satisfies $\mathfrak{R}(\boldsymbol{c}, \boldsymbol{m})_{l,n} = c_{l,n} + m_{l,n} - c_{l-1,n} - m_{l,n-1}$, $l = 1, \cdots, ii\,; n = 1, \cdots, jj$, and $c_{0,n} = m_{l,0} = c_{ii,n} = m_{l,jj} \equiv 0$. $\mathfrak{R}^{\mathrm{T}}$ is an operation that satisfies $\mathfrak{R}^{\mathrm{T}}(\boldsymbol{E}) = (\boldsymbol{c}, \boldsymbol{m})$, where $c_{l,n} = E_{l,n} - E_{l+1,n}$, $l = 1, \cdots, ii - 1, n = 1, \cdots, jj$, $m_{l,n} = E_{l,n} - E_{l,n+1}$, $l = 1, \cdots, ii, n = 1, \cdots, jj - 1$.

U_{y} means doing an orthogonal operation on the set y, and the meaning of U_O is similar to U_{y}. For example, if $\mathrm{y} = Q_{n_1,n_2}$, the calculation is

$$U_{Q_{n_1,n_2}}(\boldsymbol{E})_{l,n} = \begin{cases} n_1 & E_{l,n} < n_1 \\ E_{l,n} & n_1 \leq E_{l,n} \leq n_2\,, \\ n_2 & E_{l,n} > n_2, \end{cases} \tag{18}$$

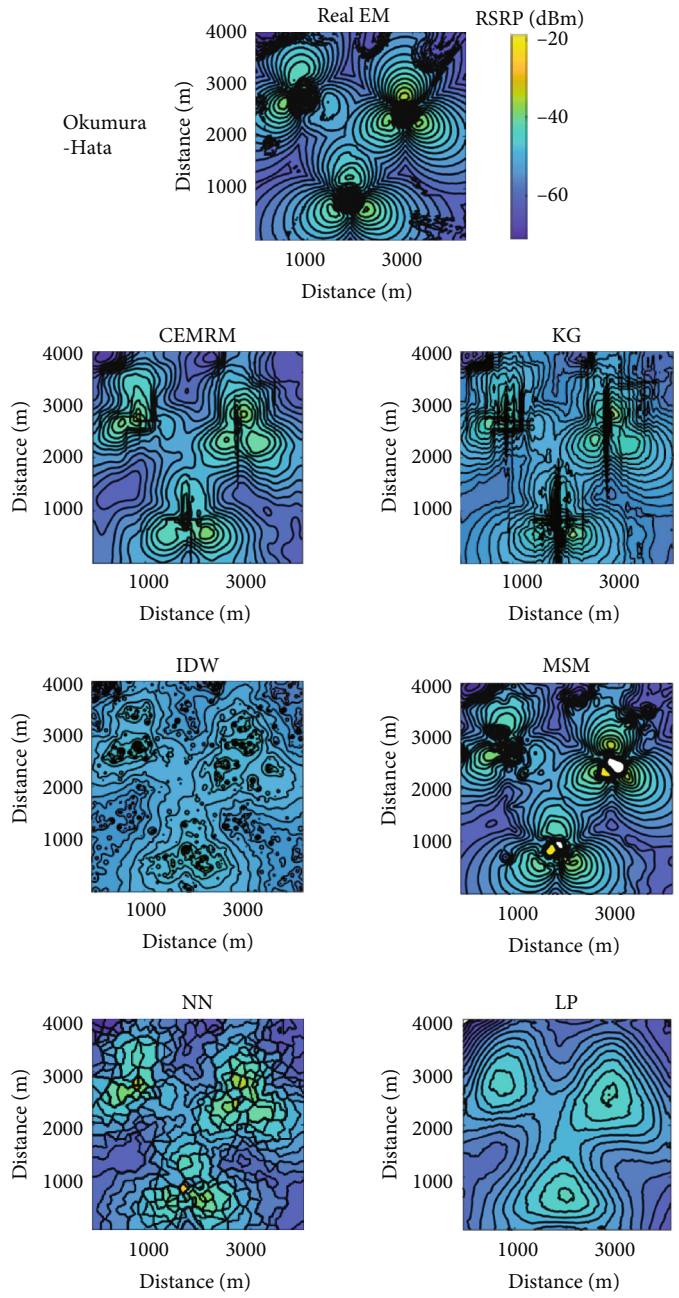

Figure 3: The reconstruction EM results of the proposed method and other five algorithms in the scenario of the Okumura-Hata model.

where Q_{n_1,n_2} is defined as

$$Q_{n_1,n_2}(\boldsymbol{E}) = [n_1 \le E_{l,n} \le n_2, \forall l, n]. \tag{19}$$

4. Simulation Results

4.1. Indicator Description. We use four indicators to demonstrate advantages of the proposed method, which are the root mean square error (RMSE), determination coefficient (R^2), robustness, and quality of the reconstructed EM (QoM).

RMSE represents the average error between the reconstructed ED and real ED. If the RMSE is small, the result is accurate. Equation (20) shows the calculating procedure of RMSE. R^2 represents the similarity of the data distribution between the reconstructed ED and real ED. If the value is high, the data distribution of the reconstructed ED is similar to that of the real ED. That is, the reconstructed EMs are realistic. Equation (21) shows the calculating procedure of R^2. What we study is the EM reconstruction with a small number of sensing nodes. Therefore, if the available sensing nodes decrease, the effect of the method should not decrease

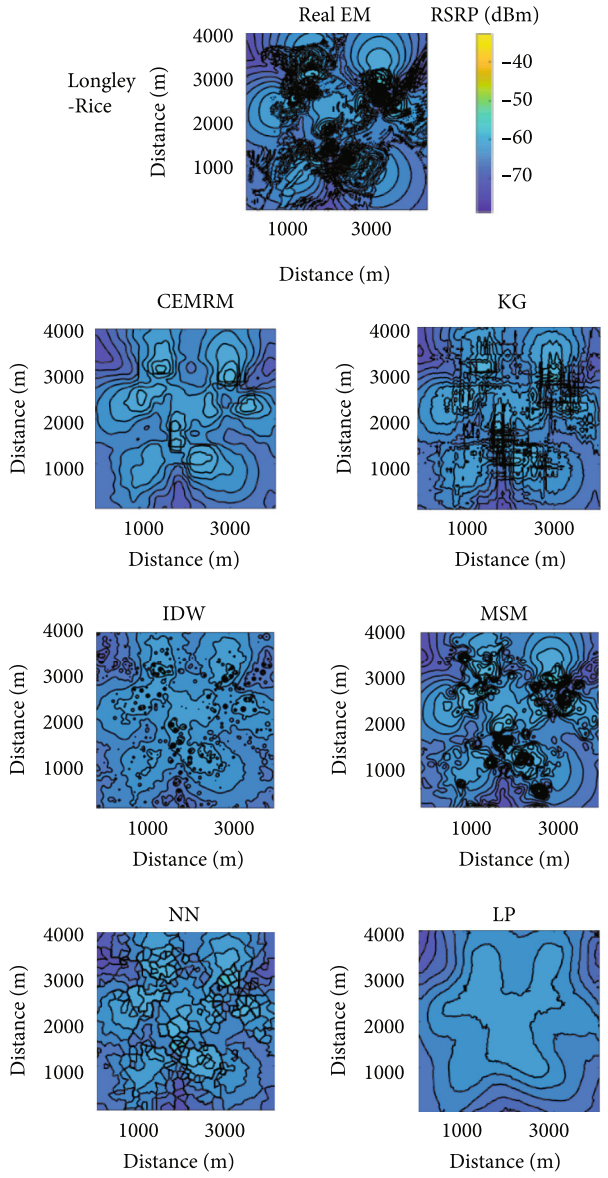

Figure 4: The reconstruction EM results of the proposed method and other five algorithms in the scenario of the Longley-Rice model.

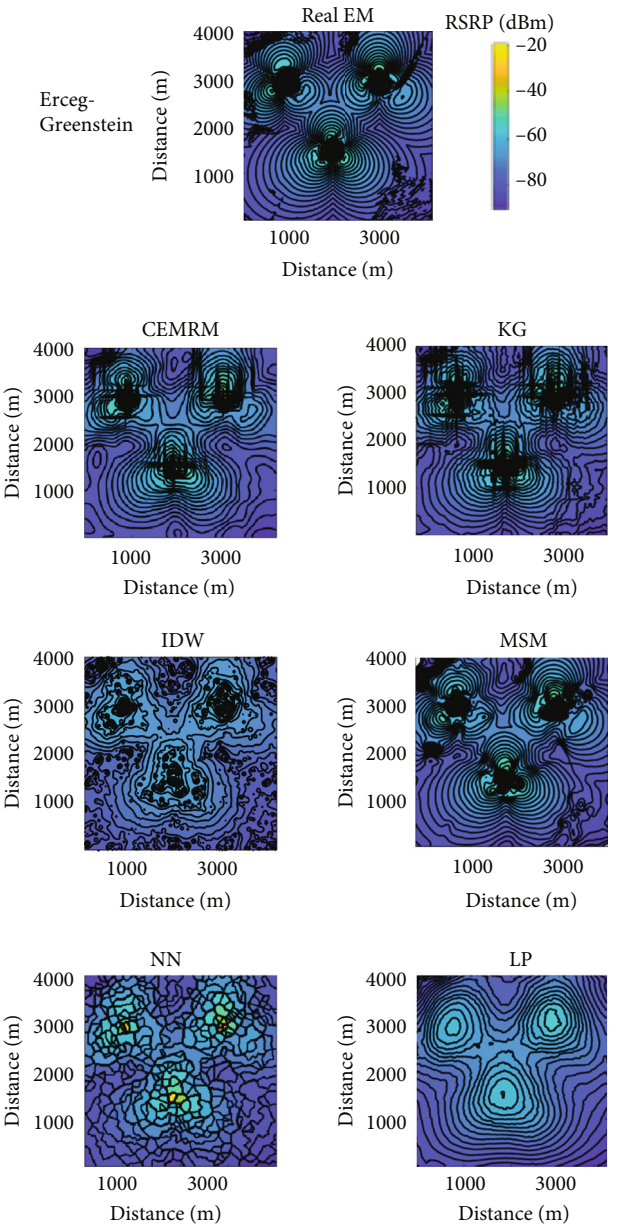

Figure 5: The reconstruction EM results of the proposed method and other five algorithms in the scenario of the Erceg-Greenstein model.

too much. That is, the method needs a good robustness. The robustness is defined as the changing range of the RMSE when the ratio of sensing nodes to the total number of ED decreases from 10% to 2%. QoM is mainly judged according to the bull's eye, the similarity of isomagnetic lines between the reconstructed result and the real EM. The RMSE and R^2 are given by

$$\mathrm{RMSE} = \frac{1}{ii \times jj} \sum_{l=1,n}^{ii} \sum_{l,n=1}^{jj} \left(\widehat{E_{l,n}} - E_{l,n} \right)^2, \tag{20}$$

$$\begin{aligned} \bar{E} &= \frac{1}{ii \times jj} \sum_{l=1,n}^{ii} \sum_{l,n=1}^{jj} E_{l,n}, \\ P_{\mathrm{tot}} &= \sum_{l=1,n}^{ii} \sum_{l,n=1}^{jj} \left(E_{l,n} - \bar{E} \right)^2, \\ P_{\mathrm{res}} &= \sum_{l=1,n}^{ii} \sum_{l,n=1}^{jj} \left(\widehat{E_{l,n}} - \bar{E} \right)^2, \\ R^2 &= 1 - \frac{P_{\mathrm{res}}}{P_{\mathrm{tot}}}, \end{aligned} \tag{21}$$

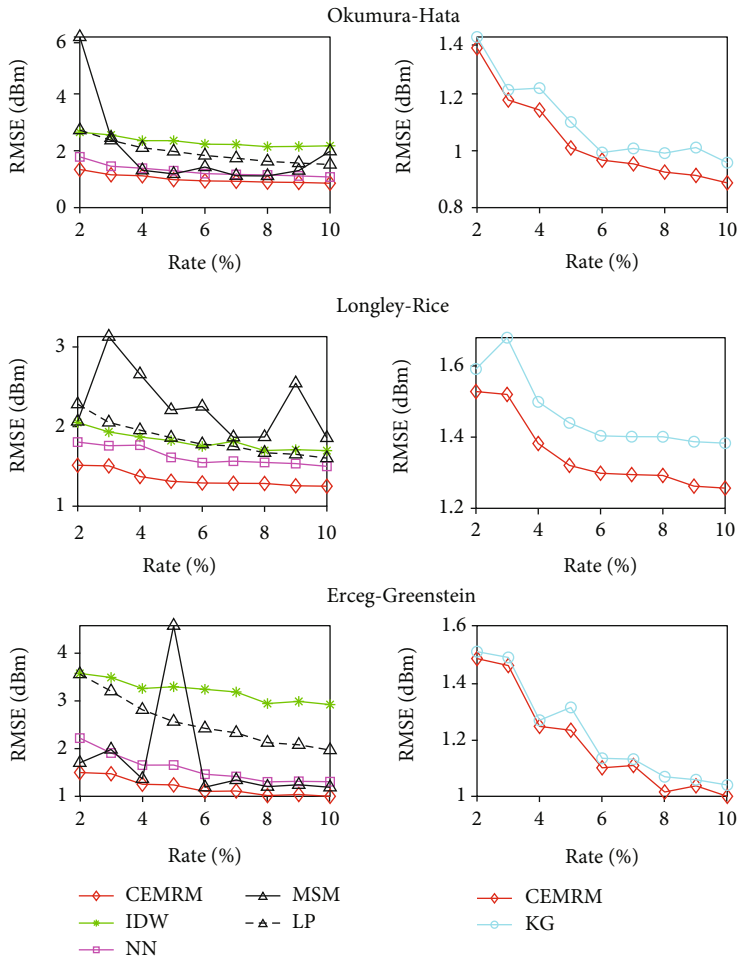

Figure 6: The RMSE results of the reconstructed EMs when the ratio of sensing nodes to the total number of ED decreases from 10% to 2%. IDW in [8], KG in [7], and MSM, NN, and LP in [22].

Table 2: R^2 of reconstruction EM results when the ratio of sensing nodes to the total number of ED is 2%.

Type	CEMRM	KG	IDW	MSM	LP	NN
Okumura-Hata	0.9539	0.9512	0.8198	0.0776	0.8097	0.9183
Longley-Rice	0.8398	0.8264	0.7040	0.7002	0.6330	0.7713
Erceg-Greenstein	0.9748	0.9739	0.8499	0.9671	0.8512	0.9433

where $\bar{E}$ is the average value of the real ED, $E_{l,n}$ is the (l, n)th real electromagnetic datum, $\widehat{E_{l,n}}$ is the corresponding reconstructed electromagnetic datum, P_{res} is the residual sum of squares, and P_{tot} is the total sum of squares.

4.2. Results and Analyses. Three base stations are arranged in an area of 4000 m × 4000 m, and the reference signal receiving power data of the long-term evolution (LTE) mobile communication network in this area are used as the experimental data. The data are generated by the currently highly recognized software Atoll, and the landform of Brussels are taken into account. The Okumura-Hata model, Longley-Rice model, and Erceg-Greenstein model are adopted as the propagation models. The frequency of electromagnetic signal is 2110 MHz, and the bandwidth is 10 MHz. The equivalent antenna height of base stations is set to 30 m, and that of detection equipments is 1.5 m. The extended matrix of the Longley-Rice model is set to 5500 m, and that of other models is set to 7000 m. All main matrices of three models are set to 4000 m. Other settings remain the original settings. The total number of the ED is 40000. The area is divided into four parts, and 200 low-cost sensing nodes are randomly deployed in each part, the ratio of sensing nodes to the total number of ED is 2%. The experimental platform is based on core i9, the software used is MATLAB R2020b, Atoll 2.8.0, Surfer 14.

If the terrain of the target area doesn't change drastically, the Okumura-Hata model is applicable. If the terrain of the target area changes drastically, the Longley-Rice model is applicable; the Erceg-Greenstein model is applicable for scenarios with shadowing. To obtain convincing results and decrease the redundant work, the abovementioned models are used.

Table 1 gives the average running time of the proposed FSSAMP and SAMP. It is seen that the average running time of FSSAMP is 7.08% accounting for that of SAMP, the proposed FSSAMP is faster than SAMP.

In order to prove the advantages of the proposed CEMRM, we adopt the modified shepard's method (MSM), KG, IDW, LP, and NN to reconstruct the EMs. What we study is the EM reconstruction in the noncooperation environment, the information of electromagnetic environment, especially the propagation models, cannot be obtained, so the indirect methods are not achievable.

Figures 3–5 show the reconstruction EM results in the different scenarios of three typical propagation models. From the three figures, it is seen that the results of IDW have lots of bull's eyes, the isomagnetic lines are greatly different from those of the real EMs; the results of MSM have fewer bull's eyes than those of IDW, there are two big white holes in the result; the results of NN have few bull's eyes, but the results are not continuous, which are different from the real EMs; the results of LP have few bull's eyes, but the results contain little changing information of electromagnetic wave, which are different from the real EMs; the results of KG have few bull's eyes, but the results cannot express the information at the locations close to base stations; the results of CEMRM have few bull's eyes, the results can express the information at the locations close to base stations, the results of CEMRM are more similar to real EMs than KG. To sum up, the QoM of CEMRM is better than that of any other algorithm mentioned above.

Figure 6 shows the changing situation in RMSE when the ratio of sensing nodes to the total number of ED decreases from 10% to 2%. It is obviously that the proposed CEMRM has the lowest RMSE in all situations. The average changing range in RMSE of the proposed CEMRM is 0.4264, the second smallest. The average changing range in RMSE of KG is 0.3887, which is the smallest. Compared with KG, the change of the proposed CEMRM in RMSE is more stable than that of KG. After comprehensive consideration, the proposed CEMRM has the better robustness than any other five algorithms.

Table 2 gives the result of R^2 between the reconstructed ED and real ED, and the ratio of sensing nodes to the total number of ED is 2%. From Table 2, it can be clearly seen that the R^2 of the results obtained by CEMRM is the largest, so the distribution of the reconstructed ED obtained by CEMRM is the most similar to the real ED.

From the comprehensive consideration of RMSE, R^2, robustness, QoM, it can be concluded that the effect of CEMRM is better than those of the existing KG, IDW, NN, LP, and MSM. The proposed CEMRM is promising to achieve the efficient application of spectrum resources and green communications in various fields [23, 24].

5. Conclusions

In order to obtain the complete and accurate ED with limited sensing nodes in the noncooperation situation, we proposed a new and practical scheme using EMs and a small number of sensing nodes, and an accurate EM reconstruction method, called CEMRM. After obtaining the incomplete sampled ED from sensing nodes, the proposed CEMRM can reconstruct the complete and accurate ED and build realistic EMs. The required minimum number of sensing nodes accounting for the total number of ED is just 2%. Compared to the existing methods of reconstructing the EMs, the proposed CEMRM remains better robustness against the decreasing of sensing nodes and obtains more accurate ED and EMs. The proposed scheme makes a good trade-off between the number of sensing nodes and accuracy of the obtained ED, and the obtained EMs can provide great support for assessing spectrum resources utilization. What we studied is helpful for green communications, high-efficiency spectrum resources utilization, and so on.

Data Availability

There are no available data.

Conflicts of Interest

The authors declare that they have no conflicts of interest.

Acknowledgments

This work was supported in part by the National Natural Science Foundation of China under grant 61971473.

References

[1] M. Liu, C. Liu, M. Li, Y. Chen, S. Zheng, and N. Zhao, "Intelligent passive detection of aerial target in space-air-ground integrated networks," *China Communications*, vol. 19, no. 1, pp. 52–63, 2022.

[2] M. Liu, B. Li, Y. Chen et al., "Location parameter estimation of moving aerial target in space-air-ground integrated networks-based IoV," *IEEE Internet of Things Journal*, vol. 9, no. 8, pp. 5696–5707, 2022.

[3] A. C. Suarez Rodriguez, N. Haider, Y. He, and E. Dutkiewicz, "Network optimisation in 5G networks: a radio environment map approach," *IEEE Transactions on Vehicular Technology*, vol. 69, no. 10, pp. 12043–12057, 2020.

[4] P. Gajewski, "Propagation models in radio environment map design," in *2018 Baltic URSI Symposium (URSI)*, pp. 234–237, Poznan, Poland, May 2018.

[5] M. Pesko, T. Javornik, A. Kosir, M. Stular, and M. Mohorcic, "Radio environment maps: the survey of construction methods," *KSII Transactions on Internet and Information Systems*, vol. 8, no. 11, pp. 3789–3809, 2014.

[6] H. B. Yilmaz and T. Tugcu, "Location estimation-based radio environment map construction in fading channels," *Wireless Communications and Mobile Computing*, vol. 15, no. 3, pp. 561–570, 2015.

[7] S. N. Lophaven, H. B. Nielsen, and J. Søndergaard, "DACE-A MATLAB kriging toolbox," IMM-TR-2002-12, Technical University of Denmark, 2002.

[8] M. Suchański, P. Kaniewski, J. Romanik, E. Golan, and K. Zubel, "Radio environment maps for military cognitive networks: density of small-scale sensor network vs. map quality," *EURASIP Journal on Wireless Communications and Networking*, vol. 2020, no. 1, 2020.

[9] X. Liu, F. Chen, and C. Lu, "Robust prediction and outlier detection for spatial datasets," in *12th IEEE International Conference on Data Mining*, pp. 469–478, Brussels Belgium, Dec. 2012.

[10] H. Xia, S. Zha, J. Huang, and J. Liu, "Radio environment map construction by adaptive ordinary kriging algorithm based on affinity propagation clustering," *International Journal of Distributed Sensor Networks*, vol. 16, no. 5, 2020.

[11] V. Fibriyani and N. Chamidah, "Prediction of inflation rate in Indonesia using local polynomial estimator for time series data," *Journal of Physics: Conference Series*, vol. 1776, no. 1, 2021.

[12] Y. Ruan, Y. Xiao, Z. Hao, and B. Liu, "A nearest-neighbor search model for distance metric learning," *Information Sciences*, vol. 552, pp. 261–277, 2021.

[13] J. Talvitie, M. Renfors, and E. S. Lohan, "Distance-based interpolation and extrapolation methods for RSS-based localization with indoor wireless signals," *IEEE Transactions on Vehicular Technology*, vol. 64, no. 4, pp. 1340–1353, 2015.

[14] K. Sato and T. Fujii, "Kriging-based interference power constraint: integrated design of the radio environment map and transmission power," *IEEE Transactions on Cognitive Communications and Networking*, vol. 3, no. 1, pp. 13–25, 2017.

[15] J. Li, Z. Gao, and Z. Pei, "The radio environment map parameter estimation using kriging method based on propagation model," *Journal of Computational Information Systems*, vol. 11, no. 20, pp. 7607–7616, 2015.

[16] K. Tsukamoto, M. Kitsunezuka, and K. Kunihiro, "Highly accurate radio environment mapping method based on transmitter localization and spatial interpolation in urban LoS/NLoS scenario," in *2018 IEEE Topical Conference on Wireless Sensors and Sensor Networks*, pp. 5–7, Anaheim, CA, USA, Jan. 2018.

[17] J. Lu, S. Zha, J. Huang, P. Liu, G. Chen, and S. Xu, "The iterative completion method of the spectrum map based on the difference of measurement values," in *2018 IEEE 3rd International Conference on Signal and Image Processing*, pp. 255–259, Shenzhen, China, Jul. 2018.

[18] Z. Lin, M. Lin, T. de Cola, J.-B. Wang, W.-P. Zhu, and J. Cheng, "Supporting IoT with rate-splitting multiple access in satellite and aerial-integrated networks," *IEEE Internet of Things Journal*, vol. 8, no. 14, pp. 11123–11134, 2021.

[19] J. Wang, R. Chen, J. Huang, F. Shu, Z. Chen, and G. Min, "Multiple-antenna spectrum sensing method with random arrivals of primary users," *IEEE Transactions on Vehicular Technology*, vol. 67, no. 9, pp. 8978–8983, 2018.

[20] T. T. Do, L. Gan, N. Nguyen, and T. D. Tran, "Sparsity adaptive matching pursuit algorithm for practical compressed sensing," in *Asilomar Conference on Signals, Systems and Computers*, pp. 581–587, Pacific Grove, CA, USA, Oct. 2008.

[21] A. Beck and M. Teboulle, "Fast gradient-based algorithms for constrained total variation image denoising and deblurring problems," *IEEE Transactions on Image Processing*, vol. 18, no. 11, pp. 2419–2434, 2009.

[22] "Surfer14," 2017, https://www.goldensoftware.com/products/surfer.

[23] Z. Lin, H. Niu, K. An et al., "Refracting RIS aided hybrid satellite-terrestrial relay networks: Joint beamforming design and optimization," *IEEE Transactions on Aerospace and Electronic Systems*, 2022.

[24] Z. Lin, M. Lin, J.-B. Wang, T. de Cola, and J. Wang, "Joint beamforming and power allocation for satellite-terrestrial integrated networks with non-orthogonal multiple access," *IEEE Journal of Selected Topics in Signal Processing*, vol. 13, no. 3, pp. 657–670, 2019.